

## ARTICLE

## OPEN



# Rupture stress of liquid metal nanoparticles and their applications in stretchable conductors and dielectrics

Yang Liu<sup>1,2</sup>, Xinyi Ji<sup>1</sup>✉ and Jiajie Liang<sup>1,3,4</sup>✉

Few works had systematically investigated the relationship between the rupture stress of the oxide shell and the diameter of liquid metal nanoparticles (LMNPs). Here, we fabricated a series of elastomer/LMNPs composites, which were based on various polyurethanes with different shore hardness and LMNPs with different diameters, to systematically study the rupture stress of LMNPs. We established a reliable and guidable relationship between the stress-strain curves of elastomers with different shore hardness and rupture stress of LMNPs with various diameters by both experiments and numerical calculations. Based on this guidance, we can facilely prepare stretchable conductors with remarkable stretchability and conductivity (i.e.,  $24,130 \text{ S} \cdot \text{cm}^{-1}$  at 500% strain) and stretchable dielectrics with excellent stretchability and permittivity (i.e., dielectric constant of 76.8 with 580% strain) through controlling the shore hardness of elastomers and diameter of LMNPs. This work will facilitate the systematic study of LMNPs and expand their use in stretchable electronics.

*npj Flexible Electronics* (2021)5:11; <https://doi.org/10.1038/s41528-021-00108-w>

## INTRODUCTION

Stretchable functional materials have attracted much attention recently due to their wide use in deformable electronics ranging from robotic sensory skins and wearable communication electronics to bio-integrated devices<sup>1–4</sup>. The most promising approach for the preparation of stretchable functional materials is to embed functional fillers into elastomers, thus integrating the complementary advantages of the inorganics' functionality with the elastomers' mechanical stretchability<sup>5–7</sup>. Unfortunately, the reported mechanical performance of these composites decreases with increasing loading of inorganic fillers due to their mechanical stiffness and brittleness<sup>8–12</sup>. This has motivated an extensive research effort focused on the development and use of functional materials with large stretchability and low modulus.

Liquid metal (LM), particularly eutectic gallium indium (EGaIn), appear to be the most promising candidate for resolving the trade-off between functionality and stretchability<sup>7,13–17</sup>. On the one hand, EGaIn possesses properties of fluids such as negligible vapor pressure, low viscosity ( $2 \text{ mPa} \cdot \text{s}$ )<sup>18</sup>, low melting point ( $\sim 14.5 \text{ }^\circ\text{C}$ )<sup>15</sup>, high surface tension ( $\sim 550 \text{ mN/m}$ )<sup>19</sup>, liquid-like conformability, and self-repairing ability at room temperature<sup>20,21</sup>. Recently, Parida et al. developed an extremely stretchable and healable conductor based on EGaIn by exploiting its fluidity property<sup>22</sup>. On the other hand, EGaIn also has many metallic characteristics such as high thermal conductivity ( $\lambda = 26.4 \text{ W m}^{-1} \text{ K}^{-1}$ ,  $T = 30 \text{ }^\circ\text{C}$ )<sup>23</sup> and electrical conductivity ( $\sigma = 34,000 \text{ S} \cdot \text{cm}^{-1}$ )<sup>14</sup>. Exploiting its metallic properties, some researchers have fabricated stretchable electrodes through the formation of EGaIn conductive channels inside the composites. For example, Wang et al. reported an intrinsically stretchable conductor with a working range of  $\sim 1,000\%$ , initial conductivity of  $8,331 \text{ S} \cdot \text{cm}^{-1}$ , and high mechanical stability that was prepared by mixing ethylene vinyl acetate copolymer, silver flakes, and LM nanoparticles (LMNPs)<sup>24</sup>. Tang et al. obtained printable, stretchable

( $\sim 500\%$ ), highly conductive ( $\sim 2,316 \text{ S} \cdot \text{cm}^{-1}$ ), and durable electrodes for which electrical pathways were formed by peeling off the polymers from the patterned EGaIn particles<sup>25</sup>. Yang et al. fabricated stretchable energy-harvesting tactile interactive interface with high performance using mechanical sintered, LM-based stretchable electrodes<sup>26</sup>. Moreover, LMNPs were also adopted to construct dielectrics. Bartlett et al. incorporated 50% by volume (hereafter referred to as 50 vol%) of EGaIn droplets into elastomers to create all-soft dielectric films. The film with 50 vol% LMNPs inclusion could endure 600% strain and showed high dielectric constant of 42 across the frequency range from 1 to 200 kHz<sup>18</sup>.

The structure of insulating solid shell and conductive liquid core for the LMNPs enables their use in the fabrication of stretchable conductors and stretchable dielectrics. In the typical synthesis, bulk EGaIn is ruptured into nanoparticles via tip sonication<sup>27,28</sup>. The stretchable conductors or dielectrics are obtained by mixing LMNPs with hyperelastic elastomers<sup>28,29</sup>. Although the sizes of the synthesized LMNPs vary, all LMNPs have similar core-shell structure consisting of a spontaneously formed dielectric solid  $\text{Ga}_2\text{O}_3$  shell and highly conductive liquid EGaIn core<sup>14,30–32</sup>. However, the integrity of the outer dielectric  $\text{Ga}_2\text{O}_3$  shells used in stretchable conductors and dielectrics is quite different. In the LM-based stretchable conductors,  $\text{Ga}_2\text{O}_3$  shells are broken and the encapsulated EGaIn flows out to coalesce, providing a dynamic and robust electrical pathway<sup>5,28</sup>. By contrast,  $\text{Ga}_2\text{O}_3$  shells remain intact in the LM-based stretchable dielectrics. The  $\text{Ga}_2\text{O}_3$  shells serve as powerful dielectric barriers between neighboring LMNPs<sup>18,33</sup>. Based on the above discussion, the integrity of the outer dielectric  $\text{Ga}_2\text{O}_3$  shells determines the LMNPs functionality and applications. However, few works had systematically investigated the relationship between the rupture stress of the oxide shell and the diameter of LMNPs<sup>5,28,29,34</sup>.

In this work, we fabricated a series of elastomer/LMNPs composites, which were based on a range of polyurethane (PU)

<sup>1</sup>School of Materials Science and Engineering, National Institute for Advanced Materials, Nankai University, Tianjin, PR China. <sup>2</sup>College of Light Industry Science and Engineering, Tianjin University of Science and Technology, Tianjin, PR China. <sup>3</sup>Key Laboratory of Functional Polymer Materials of Ministry of Education, College of Chemistry, Nankai University, Tianjin, PR China. <sup>4</sup>Tianjin Key Laboratory of Metal and Molecule-Based Material Chemistry and Collaborative Innovation Center of Chemical Science and Engineering (Tianjin), Nankai University, Tianjin, PR China. ✉email: xyji06@nankai.edu.cn; liang0909@nankai.edu.cn

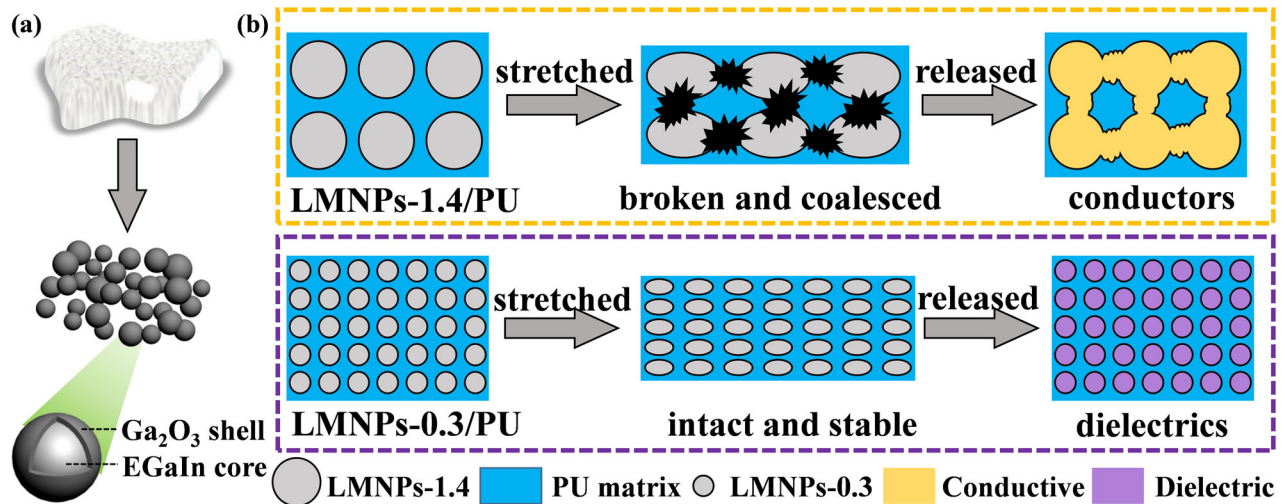


**Fig. 1 Design of LM-based stretchable conductors and dielectrics.** **a** The LMNPs preparation process and core-shell structure. **b** Schematic illustration of morphology changes of LMNPs-1.4 and LMNPs-0.3 applied in stretchable conductors and dielectrics. LMNPs-1.4/PU or LMNPs-0.3/PU samples are obtained by mixing LMNPs-1.4 or LMNPs-0.3 with corresponding PU, respectively.

matrix with different shore hardness and LMNPs with different diameters, to systematically study the rupture stress of LMNPs. Furthermore, we established a reliable and guidable relationship between the stress-strain curves of elastomers with different shore hardness and rupture stress of LMNPs with various diameters by both experiments and numerical calculations. Based on this guidance, we can facilely prepare stretchable conductors with remarkable stretchability and conductivity (i.e., 24,130 S·cm<sup>-1</sup> at 500% strain) and stretchable dielectrics with excellent stretchability and permittivity (i.e., dielectric constant of 76.8 with 580% strain) through controlling the shore hardness of elastomer and diameter of LMNPs.

## RESULTS AND DISCUSSION

### Theoretical calculation and experimental verification

In the experiments performed to measure the LMNPs activation stress, the direct application of stress to the LMNPs is inconvenient. Therefore, we adopted elastic PU to supply the stress and read the loaded stress from its stress-strain curve. The typical experimental procedure was as follows: First, EGaIn was broken up into nanoparticles via tip sonication<sup>28</sup>. A dielectric Ga<sub>2</sub>O<sub>3</sub> shell with a thickness of 0.5–3 nm forms spontaneously upon the exposure of the nanoparticles to air as shown in Fig. 1a and revealed by TEM (Supplementary Fig. 1)<sup>14,35</sup>. The particle size can be tuned from 1.8 μm to 0.3 μm by prolonging the sonication time from 0.5 min to 30 min as shown in Supplementary Fig. 2<sup>27,36</sup>. Specifically, LMNPs with different average diameters were denoted as LMNPs-x, where x represented the average diameter (μm) of the obtained LMNPs after sonication for certain time. Commercially available PU with different shore hardness (85PU, 65PU, and 55PU where the number represents its shore hardness) was selected as the elastic matrix and stress supplier. Following material selection, all LMNPs/PU composites were fabricated by screen printing. Unless otherwise noted, the stretchable composites were denoted as yLMNPs-x/zPU (for instance, 80%LMNPs-1.4/85PU means 80 vol% LMNPs-1.4 dispersed in 85PU matrix). The composites were fabricated with a length, width, and thickness of about 20 mm, 3.5 mm, and 20 μm, respectively. All the samples were mounted on a motorized linear stage connected to a Keithley 2000 digital multimeter used to monitor the resistance change. Displacement tests coupling with electrical measurements were performed simultaneously at a constant strain rate of 0.1%·s<sup>-1</sup>. We assumed that the specimen was dielectric until the Keithley 2000 digital

multimeter could detect its resistance and recorded the mechanical strain as the specimen activation strain. The LMNPs activation stress was obtained from the stress-strain curve of the corresponding PU. Based on the previous reports<sup>27,34</sup>, the force for breaking the particles was calculated as:

$$f = \frac{d^2}{D^2} \times F \times P \quad (1)$$

where F is the measured force applied by the circular punch, f is the force for breaking the particles, D is the diameter of the circular polystyrene punch, d is the average particle diameter, and P is the three-dimensional packing factor of the particles. When the sample is stretched to the activation strain, the activation stress is calculated as

$$S = \frac{6.16d + 3.04 \times 10^{-7}}{\pi d^2} \quad (2)$$

where S is the activation stress of LMNPs. More details could be obtained in Supplementary Note 1. Fig. 2a shows the activation stress plotted as a function of LMNPs diameter (red solid curve) obtained according to Eq. (2). To facilitate comparison, the stress-strain curves of various PUs are also plotted. As depicted in Fig. 2a, the activation stress of LMNPs is inversely proportional to their size so that larger LMNPs break more easily than smaller LMNPs. To clearly show the shell integrity of the LMNPs of various sizes under different stress, Fig. 2a is divided into two regions by the activation stress–LMNPs diameter curve. In the orange area, LMNPs will rupture under the overloaded stress and the leaked EGaIn will form a continuous network inside the composite. However, in the purple area, the external stress does not reach the activation stress of the corresponding LMNPs, so that their shells remain intact and act as electron barriers. Taking LMNPs-1.4 and LMNPs-0.3 as examples, the activation stress of LMNPs-1.4 is 1.5 × 10<sup>6</sup> Pa and once the applied stress exceeds this value, the LMNPs-1.4 become conductive. On the other hand, the activation stress of LMNPs-0.3 (9.5 × 10<sup>6</sup> Pa) is much higher than that of LMNPs-1.4, indicating that LMNPs-0.3 are more robust than LMNPs-1.4. When the external stress is lower than 9.5 × 10<sup>6</sup> Pa, the LMNPs-0.3 remain insulating and are suitable for use in dielectric composites.

Two factors determine the integrity of the Ga<sub>2</sub>O<sub>3</sub> shells: (1) the inherent activation stress of LMNPs; and (2) the external applied stress. The accuracy of Eq. (2) is validated by varying the size of LMNPs and the modulus of the PU matrix. As revealed in Fig. 2b, the experimental activation strains of 50%LMNPs-1.4/85PU and

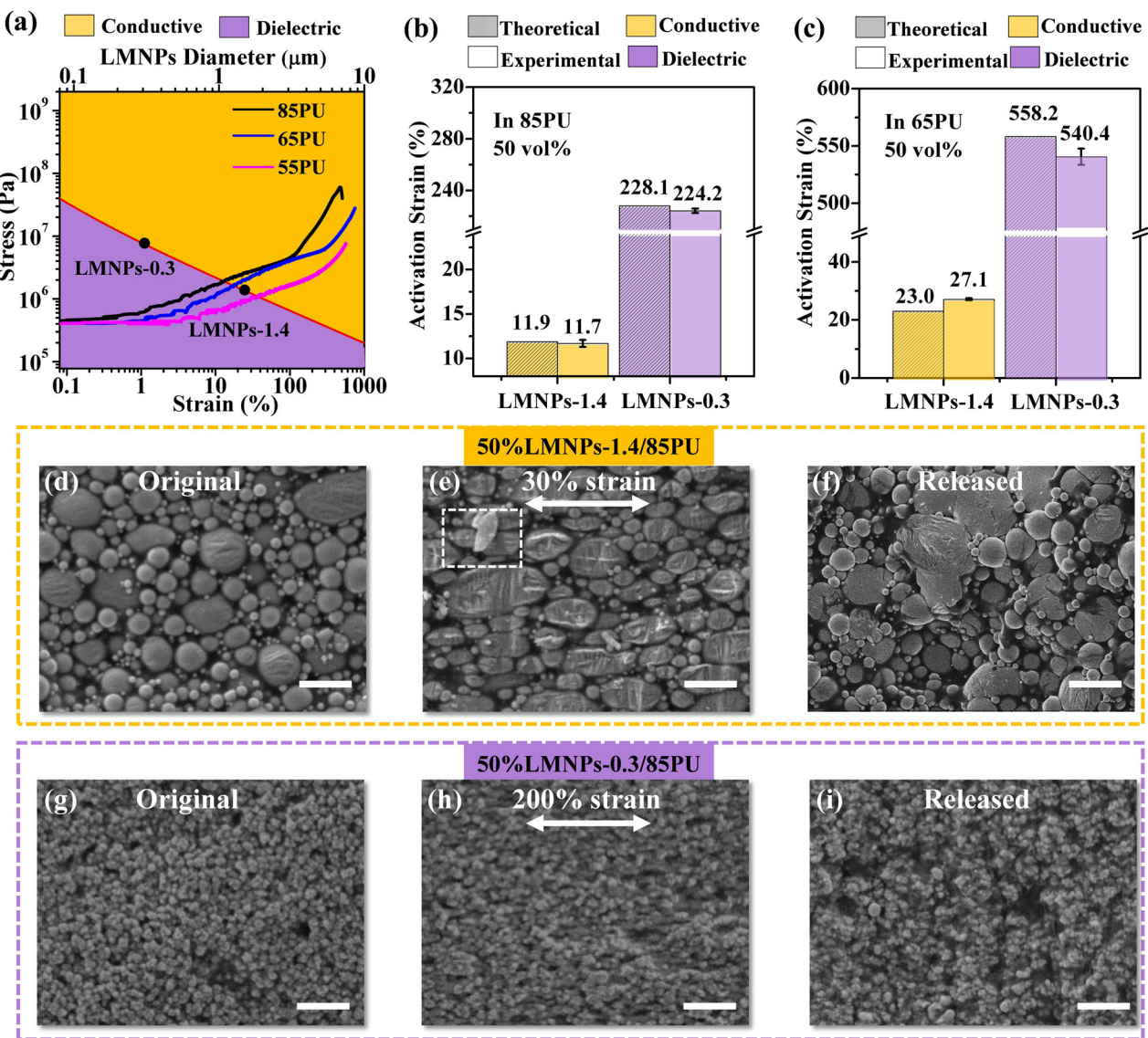


**Fig. 2 Verification of calculated results.** **a** Stress–strain curves of various PU coupled with calculated LMNPs activation stress. Theoretical and experimental activation strain of **b** 50%LMNPs-1.4/85PU and 50%LMNPs-0.3/85PU and **c** 50%LMNPs-1.4/65PU and 50%LMNPs-0.3/65PU. The error bars show the standard deviation. Top view SEM images of 50%LMNPs-1.4/85PU under **d** original state, **e** 30% strain, and **f** relaxed state and 50%LMNPs-0.3/85PU under **g** original state, **h** 200% strain, and **i** relaxed state. Outflowed EGaIn is emphasized in white box with dashed lines of **e**. The scale bars in **d–i** are 4  $\mu\text{m}$ .

50%LMNPs-0.3/85PU composites were 11.7% and 224.2%; these values are almost identical to the calculated activation strain values of 11.9% and 228.1%, respectively. SEM images of 50%LMNPs-1.4/85PU and 50%LMNPs-0.3/85PU composites provided morphological insight into the LMNPs changes during the multiple steps of the stretching-releasing process. In the original state, both spherical LMNPs-1.4 and LMNPs-0.3 (Fig. 2d, g) had closed-cell geometry and were dispersed uniformly in the 85PU matrix, differing only with respect to their size. Then, the 50%LMNPs-1.4/85PU sample was stretched to 10% strain and released. The  $\text{Ga}_2\text{O}_3$  shells were not broken and inner EGaIn was still encapsulated as revealed in Supplementary Fig. 3a. After the strain was further increased to 30% (much larger than its activation strain of 11.9%), the outer  $\text{Ga}_2\text{O}_3$  shells were broken and the inner EGaIn flowed out to form electrical channels as emphasized in the white box marked by dashed lines in Fig. 2e. Finally, the EGaIn microchannels formed inside the matrix and the 50%LMNPs-1.4/85PU composites functioned as stretchable conductors after releasing back to the 0% strain state as depicted in Fig. 2f.

By contrast, 50%LMNPs-0.3/85PU composites remained insulating and endured much larger strain. As revealed in Fig. 2h, the nonconductive shells of LMNPs-0.3 were intact for the 50%LMNPs-0.3/85PU composites even under 200% strain. This is because the LMNPs-0.3 can endure stress that is as high as  $9.5 \times 10^6$  Pa and the activation strain of 50%LMNPs-0.3/85PU increased to 228.1%. Finally, the LMNPs-0.3 returned to its original spherical shape as illustrated in Fig. 2i and the 50%LMNPs-0.3/85PU composites remained insulating after releasing back to original state. However, large stress will tear the oxidized shells once the strain value exceeds 230%, in agreement with the SEM results (Supplementary Fig. 3b). These above experimental results are consistent with our calculated results and validated the effectiveness and accuracy of Eq. (2). Subsequently, 85PU was replaced by 65PU that has a much lower Young's modulus to validate the influence of the matrix modulus. As shown in Fig. 2c, the experimental activation strain increased to 27.1% and 540.4% for 50%LMNPs-1.4/65PU and 50%LMNPs-0.3/65PU, respectively, matching the corresponding calculated activation strain values

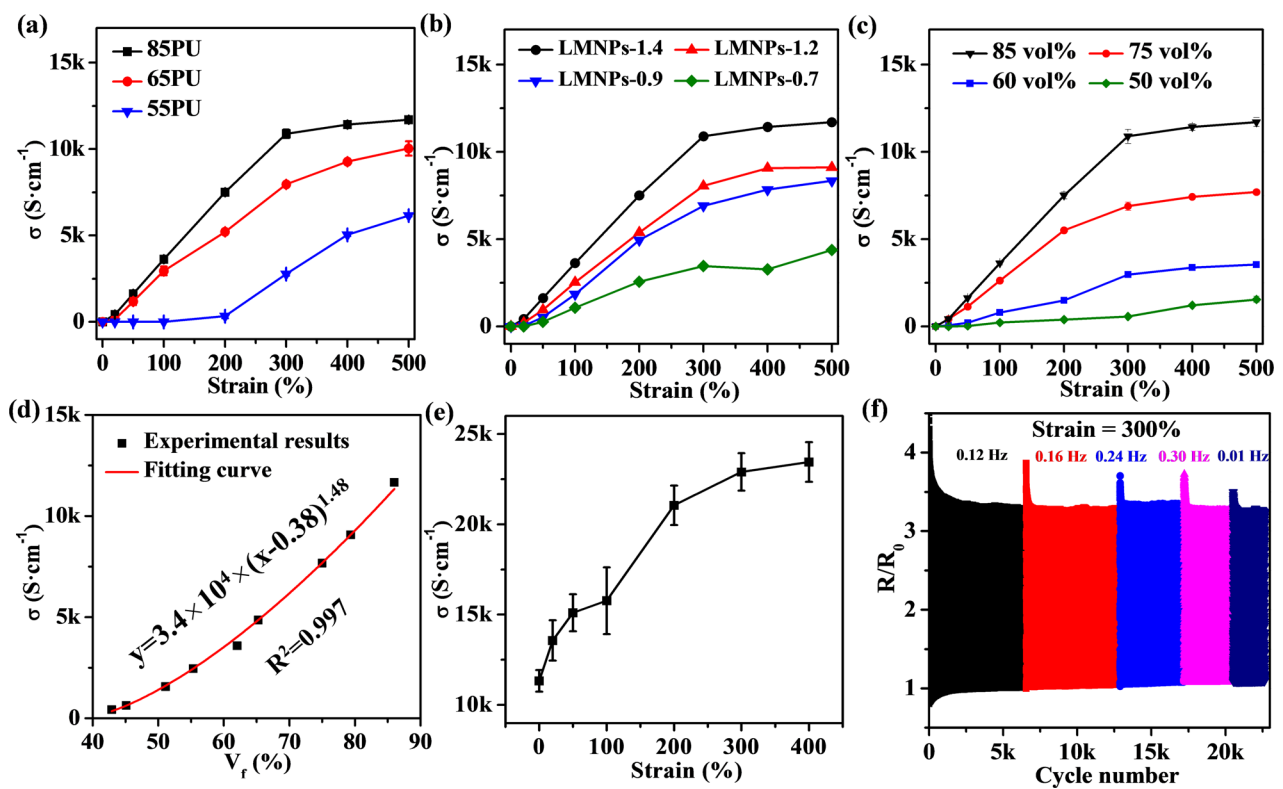


**Fig. 3 Electrical performance of LM-based stretchable conductors.** Relationship of conductivity in the releasing state (0% strain) after certain strains with **a** PU, **b** LMNPs diameters, and **c** LMNPs volume percentage. **d** Fitting of the experiment data with the percolation theory. **e** Conductivity-applied strain curve of 85%LMNPs-1.4/85PU. **f** Normalized resistance changes of 85%LMNPs-1.4/85PU subjection to 300% strain for 20,000 cycles at various rates (0.12, 0.16, 0.24, 0.30, and 0.01 Hz). The error bars show the standard deviation.

of 23.0% and 558.2%, respectively. Even though 85PU was replaced by 65PU, the activation stress values of 50%LMNPs-1.4/65PU ( $1.47 \times 10^6 \text{ Pa}$ ) and 50%LMNPs-0.3/65PU ( $9.52 \times 10^6 \text{ Pa}$ ) were essentially the same as those of 50%LMNPs-1.4/85PU ( $1.46 \times 10^6 \text{ Pa}$ ) and 50%LMNPs-0.3/85PU ( $9.53 \times 10^6 \text{ Pa}$ ), further confirming the accuracy of Eq. (2).

### LM-based stretchable conductors

The integrity of the LMNPs shells and their suitability for applications can be easily determined by the comparison of the LMNPs threshold activation stress to the stress supplied by the polymer matrix. Once the supplied stress was larger than activation stress, LMNPs became conductive fillers and were suitable for use in stretchable conductors. In the following steps, to resolve the trade-off between conductivity and stretchability, we focused our effort on the development and optimization of LM-based stretchable electrodes using these broken LMNPs. It was easily concluded from the above calculations that the modulus of the elastomer matrix and strain influenced the supplied stress while the activation stress depended solely on the diameter of LMNPs. Fig. 3a shows the obtained conductivity ( $\sigma$ ) after certain strains for the composites adopting 85PU, 65PU, and 55PU as the polymer matrix. An examination of the cross-section SEM images of the samples (Supplementary Fig. 4) shows that greater fusing area of broken LMNPs was obtained with larger strain and matrix modulus. The specimens with 85PU as the polymer matrix obtained the highest conductivity after 500% strain due to its high modulus. Furthermore, the relationship between the conductivity after certain strains and LMNPs diameter was demonstrated in Fig. 3b. As revealed in the cross-sectional SEM images of the specimens with different LMNPs diameters (Supplementary Fig. 5), the specimens containing LMNPs-1.4

obtained the highest conductivity. Further increase in the diameter (about  $1.8 \mu\text{m}$  in Supplementary Fig. 5a) will lead to poor dispersion of the LMNPs in the composites. The relationship between the sample conductivity after certain strains and amount of LMNPs is shown in Fig. 3c. It is observed that an excessive amount of LMNPs lowered the conductivity due to the insufficient PU coverage on the particles surface, while an inadequate amount of LMNPs resulted in a longer distance between the adjacent particles. Consequently, thicker matrix shells hindered the agglomeration of the particles as demonstrated in Supplementary Fig. 6.

To summarize, the 85%LMNPs-1.4/85PU specimen optimized the highest conductivity ( $11,702 \text{ S} \cdot \text{cm}^{-1}$ ). In fact, the broken LMNPs can be regarded as conductive fillers and obey the percolation theory relationship<sup>8,37</sup>

$$A = A_0(V_f - V_c)^b$$

where  $A$  and  $A_0$  denote the conductivities of the composites and bulk EGaIn, respectively, and  $V_f$ ,  $V_c$ , and  $b$  are the volume fraction of conductive fillers, the volume fraction of the percolation threshold, and the fitting exponent, respectively. As depicted in Fig. 3d, the results obtained using 0.38, 1.48, and 34,000 for  $V_c$ ,  $b$ , and  $A_0$ , respectively, in computer-aided calculation showed a good agreement with the experimental data. Additional calculation details are provided in Supplementary Note 2. The stretching state conductivity decrease is the fatal weakness that leads to device performance degradation<sup>38</sup>. Unlike for the other types of stretchable conductors, the initial conductivity of the 85%LMNP-1.4/85PU composite was  $11,702 \text{ S} \cdot \text{cm}^{-1}$  and increased gradually to  $24,130 \text{ S} \cdot \text{cm}^{-1}$  at 500% strain as revealed in Fig. 3e. This unusual phenomenon was attributed to the conformal characteristic of LM that induced an enhancement of the conductivity along the stretching direction<sup>5</sup>. Supplementary Fig. 7 shows a comparison of

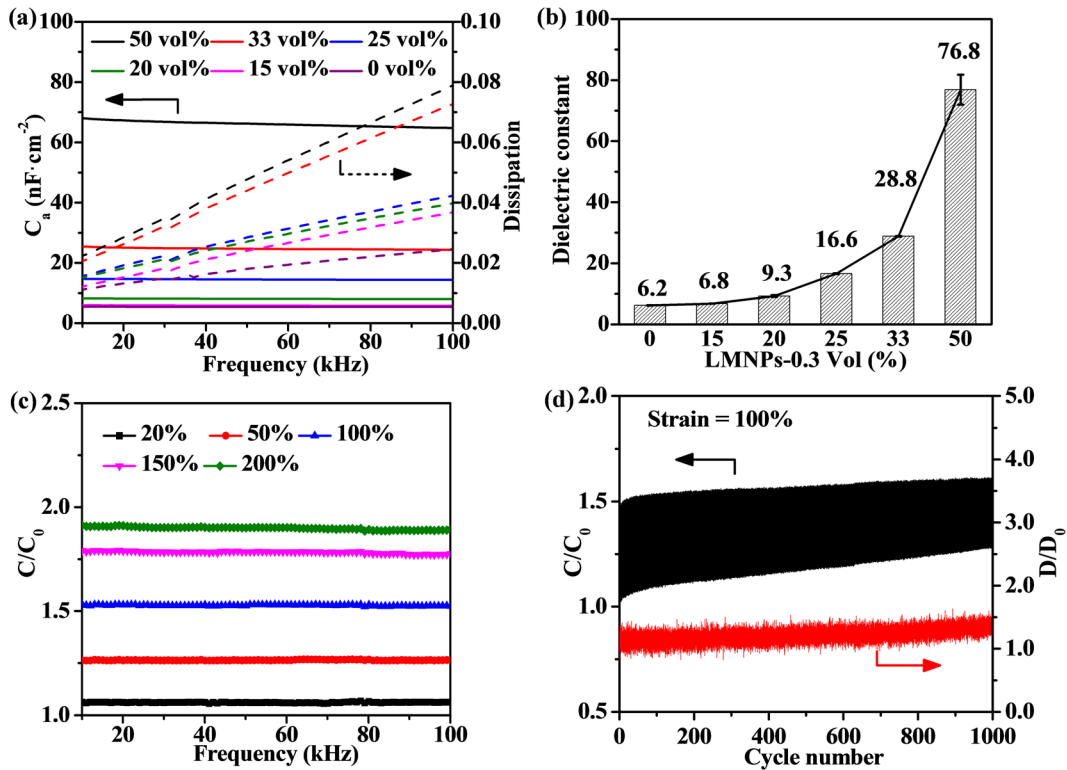


**Fig. 4 Electrical performance of LM-based stretchable dielectrics.** **a** Comparison of specific capacitance and dissipation of LMNPs-0.3/55PU with various LMNPs-0.3 volume percentage under 10–100 kHz. **b** Dielectric constant of LMNPs-0.3/55PU with various LMNPs-0.3 volume percentage under 100 kHz. The error bars show the standard deviation. **c** Normalized capacitance of 50%LMNPs-0.3/55PU subjection to various strain under 10–100 kHz. **d** Normalized capacitance and dissipation of 50%LMNPs-0.3/55PU subjection to 100% strain for 1,000 cycles.

the electrical conductivity and working range of the 85%LMNPs-1.4/85PU electrodes to other previously reported stretchable and printable conductors<sup>8–12,24,25,39–49</sup>.

To cope with challenging external environmental conditions, the reliability of stretchable electrodes at different stretching frequencies is also crucial. As shown in Fig. 3f, normalized resistance ( $R/R_0$ ) of the 85%LMNPs-1.4/85PU stretchable electrodes at 300% strain remains constant at ~3.3 as the stretching frequency increases from 0.01 to 0.30 Hz. The electrodes also showed no obvious degradation in normalized resistance (Fig. 3f) and conductivity (Supplementary Fig. 8) even after a total of 20,000 stretching-releasing cycles under 300% strain, demonstrating their mechanical robustness and reliability for practical applications. A normalized resistance change of the 85%LMNPs-1.4/85PU stretchable electrodes subjected to 200% and 100% strains at various rates is presented in Supplementary Fig. 9.

### LM-based stretchable dielectrics

The intact LMNPs can be used in the dielectric materials as specific capacitance ( $C_a$ ) and permittivity ( $\epsilon$ ) enhancing fillers on the premise of high stretchability. According to the calculations, the outer  $\text{Ga}_2\text{O}_3$  shells of LMNPs-0.3 can encapsulate EGaIn and prevent its outward flow for stresses of up to  $9.53 \times 10^6$  Pa, far more than the tensile stress of 55PU ( $5.40 \times 10^6$  Pa at 580% strain). The sample remained insulating until rupture. As plotted in Fig. 4a, the specific capacitance of the LMNPs-0.3/55PU dielectric film increased monotonically with more LMNPs-0.3 addition and reached nearly 1,200% [ $C_a$  (50%LMNPs-0.3/55PU, 100 kHz) =  $64.7 \text{ nF} \cdot \text{cm}^{-2}$ ] compared to that of the blank control [ $C_a$  (55PU, 100 kHz) =  $5.4 \text{ nF} \cdot \text{cm}^{-2}$ ]. Moreover, the dissipation ( $D$ ) of all specimens in the frequency range of 10–100 kHz was lower than 0.1, well within the threshold for dielectric functionality. The low dissipation of all specimens was attributed to the dielectric property of outside

insulating  $\text{Ga}_2\text{O}_3$  and negligible conductivity of samples<sup>50</sup>. Fig. 4b presents the dielectric constant plotted versus LMNPs-0.3 volume percentage of the LMNPs-0.3/55PU dielectric film at the frequency of 100 kHz and 0% strain. The dielectric constant increased to nearly 1,240% that of 55PU and could be easily tuned from 6.2 with 0 vol% LMNPs-0.3 to 76.8 with 50 vol% LMNPs-0.3. Furthermore, the electromechanical properties of dielectric layers are also significant parameters for the evaluation of stretchable dielectrics. Fig. 4c depicts the normalized capacitance ( $C/C_0$ ) of the 50%LMNPs-0.3/55PU dielectric films at a frequency range of 10–100 kHz under various strains. Their  $C/C_0$  values remained relatively stable within the entire measured frequency range. However,  $C/C_0$  increased monotonically with stretching and reached 1.9 at 200% strain. This phenomenon can be attributed to: (1) the expanded area and (2) the thinner dielectric layer caused by stretching.

To test the reliability of the 50%LMNPs-0.3/55PU dielectric films, we performed fatigue measurements under 100% strain for 1,000 cycles (Fig. 4d). During cyclic test, the stretching  $C/C_0$  and  $D/D_0$  values remained 1.5 and 1.3, manifesting the high stability of LMNPs-0.3 inside the dielectrics and the accurate guidance provided by the results of our calculation. The results of the electrical, electromechanical, and fatigue tests of other LMNPs-0.3/55PU samples are presented in Supplementary Fig. 10. To highlight the performance of our dielectric films, we compared the specific capacitance, dielectric constant, working range, and durability of 50%LMNPs-0.3/55PU with those of the state-of-the-art stretchable dielectrics<sup>18,51–55</sup> as shown in Supplementary Table 1.

In conclusion, we calculated the rupture stress of LMNPs with different sizes and verified the validity of the calculations through experiments. Following the guidance provided by the calculated results, we fabricated LM-based, ultra-stable, hyperelastic, and highly conductive electrodes adopting coalesced broken LMNPs-1.4. As stretchable conductors, the 85%LMNPs-1.4/85PU composites

demonstrated large stretchability (>500%) and high electrical conductivity ( $11,702 \text{ S} \cdot \text{cm}^{-1}$  at 0% strain and  $24,130 \text{ S} \cdot \text{cm}^{-1}$  at 500% strain). Moreover, we fabricated dielectric films with high permittivity and specific capacitance by using intact LMNPs-0.3. As dielectric layers, the 50%LMNPs-0.3/55PU dielectric films remained insulating under 580% strain. Specific capacitance and dielectric constant reached  $64.7 \text{ nF} \cdot \text{cm}^{-2}$  and 76.8 corresponding to enhancements of 1,200% and 1,240%, respectively, compared to blank control. Fatigue measurements revealed that the dielectric films were stable under 100% strain for 1,000 cycles. This demonstrated the high stability of LMNPs-0.3 inside the dielectrics and provided an additional confirmation of the accuracy of the guidance provided by our calculations. Taken together, these results will guide the systematic study of LM as well as advance the development of next-generation deformable electronics.

## METHODS

### Raw materials

*N,N*-dimethylformamide (Sigma Aldrich) were purchased and used without further purification. PU (85PU, 65PU, 55PU) was obtained from Yantai Wanhua Polyurethane Co. Ltd. (China). EGaIn was fabricated by mixing melted gallium and indium (75% Ga/25% In, by weight) overnight.

### Preparation of LMNPs/PU ink

LMNPs were synthesized using a tip sonicator (Hielscher UP400S, Germany). EGaIn (6 g) and DMF (150 ml) were added into 250 ml beaker and treated at 90% sonication amplitude for different time length (0.5, 1, 2, 5, 10, and 30 min) to obtain particles with the target size. Then, the LMNPs were collected by centrifugation at 4,000 rpm for 5 min. PU (1 g) was added to DMF (5 ml) and stirred for 8 h to obtain a clear solution. Finally, LMNPs/PU ink was obtained by mixing LMNPs and PU solution overnight.

### Fabrication of LMNPs/PU dielectric film

Glass slides were cleaned with ultrasonication sequentially in acetone, isopropyl alcohol, and deionized water. Nanocomposite dielectric film was coated on glass substrates using a Mayer rod, followed by drying on a hot plate at  $80^\circ\text{C}$  for 10 min. The amount of LMNPs varied from 15 to 50 vol%. The printed composite film with a thickness of  $\sim 1 \mu\text{m}$  was obtained by adjusting the concentration of the dielectric film ink. For dielectric analysis, EGaIn was deposited on the film top surface using a blunt syringe needle. Subsequently, ReoFlex elastomer was poured and cured to transfer the bottom structure from the rigid substrate. Finally, EGaIn was patterned as another electrode to obtain a stretchable parallel plate capacitor and a wire probe was placed into the EGaIn contact. At least five individual measurements were performed to characterize the dielectric film.

### Characterization

Resistance-strain and fatigue tests were carried using a motorized linear stage with a built-in controller (Zolix Inc., China) while a Keithley 2000 digital multimeter (Keithley Instruments, America) was used to simultaneously monitor the resistance change. The dielectric film capacitance and dissipation were measured using a precision LCR meter (TongHui 2338H, Changzhou Tonghui Electronic Co., Ltd.) from 10 to 100 kHz at 5 V adopting the sandwich structure mentioned above. Capacitance and dielectric constant were measured at a frequency of 100 kHz. SEM characterizations were carried out using a field-emission scanning electron microscope (JSM-7800, Japan) at an accelerating voltage of 5.0 kV. TEM images were obtained using a transmission electron microscope (JEM-2800, Japan). Electric conductivity was calculated according to the equation  $\sigma = L/(RS)$ , where  $L$  is the length of the tested sample,  $R$  is the sample resistance, and  $S$  is its cross-section area. At least five samples were tested for each conductivity value. The stress-strain curves of 85PU, 65PU, and 55PU were measured using a universal tensile testing machine (SHIMADZU TRAPEZIUM-X, Japan). The optical photographs were obtained using a Leica ICC50W camera (Leica Microsystems, Germany). Particle size statistics were obtained using Nano Measure (China) and the irregular graphic area was integrated using the Image J software (China). A 3D profiler (Filmetrics, America) was used to measure the thicknesses of the composite film. Dielectric constants were calculated from the measured

capacitances, thicknesses, and cross-section area of the electrodes. All capacitance, dielectric constant, and conductivity values were averaged from the measurements performed for at least five devices, and the error bars denote the standard deviations.

## DATA AVAILABILITY

The datasets generated and analyzed during the current study are available from the corresponding author on reasonable request.

Received: 11 January 2021; Accepted: 7 May 2021;

Published online: 27 May 2021

## REFERENCES

1. Forrest, S. R. The path to ubiquitous and low-cost organic electronic appliances on plastic. *Nature* **428**, 911–918 (2004).
2. Kim, D.-H. & Rogers, J. A. Stretchable electronics: materials strategies and devices. *Adv. Mater.* **20**, 4887–4892 (2008).
3. Leber, A. et al. Soft and stretchable liquid metal transmission lines as distributed probes of multimodal deformations. *Nat. Electron.* **3**, 316–326 (2020).
4. Wang, S. et al. Skin electronics from scalable fabrication of an intrinsically stretchable transistor array. *Nature* **555**, 83–88 (2018).
5. Fassler, A. & Majidi, C. Liquid-phase metal inclusions for a conductive polymer composite. *Adv. Mater.* **27**, 1928–1932 (2015).
6. Ma, R., Chou, S.-Y., Xie, Y. & Pei, Q. Morphological/nanostructural control toward intrinsically stretchable organic electronics. *Chem. Soc. Rev.* **48**, 1741–1786 (2019).
7. Tee, B. C. K. & Ouyang, J. Soft electronically functional polymeric composite materials for a flexible and stretchable digital future. *Adv. Mater.* **30**, 1802560 (2018).
8. Chun, K.-Y. et al. Highly conductive, printable and stretchable composite films of carbon nanotubes and silver. *Nat. Nanotechnol.* **5**, 853–857 (2010).
9. Liang, J., Tong, K. & Pei, Q. A water-based silver-nanowire screen-print ink for the fabrication of stretchable conductors and wearable thin-film transistors. *Adv. Mater.* **28**, 5986–5996 (2016).
10. Matsuhashi, N. et al. Printable elastic conductors with a high conductivity for electronic textile applications. *Nat. Commun.* **6**, 7461–7471 (2015).
11. Park, M. et al. Highly stretchable electric circuits from a composite material of silver nanoparticles and elastomeric fibres. *Nat. Nanotechnol.* **7**, 803–809 (2012).
12. Sekitani, T. et al. Stretchable active-matrix organic light-emitting diode display using printable elastic conductors. *Nat. Mater.* **8**, 494–499 (2009).
13. Dickey, M. D. Stretchable and soft electronics using liquid metals. *Adv. Mater.* **29**, 1606425 (2017).
14. Kazem, N., Hellebrekers, T. & Majidi, C. Soft multifunctional composites and emulsions with liquid metals. *Adv. Mater.* **29**, 1605985 (2017).
15. Daeneke, T. et al. Liquid metals: fundamentals and applications in chemistry. *Chem. Soc. Rev.* **47**, 4073–4111 (2018).
16. Lin, Y., Genzer, J. & Dickey, M. D. Attributes, fabrication, and applications of gallium-based liquid metal particles. *Adv. Sci.* **7**, 2000192 (2020).
17. Ren, L., Xu, X., Du, Y., Kalantar-Zadeh, K. & Dou, S. X. Liquid metals and their hybrids as stimulus-responsive smart materials. *Mater. Today* **34**, 92–114 (2020).
18. Bartlett, M. D. et al. Stretchable, high-k dielectric elastomers through liquid-metal inclusions. *Adv. Mater.* **28**, 3726–3731 (2016).
19. Chen, S., Wang, H.-Z., Zhao, R.-Q., Rao, W. & Liu, J. Liquid metal composites. *Mater.* **2**, 1446–1480 (2020).
20. Markvicka, E. J., Bartlett, M. D., Huang, X. & Majidi, C. An autonomously electrically self-healing liquid metal-elastomer composite for robust soft-matter robotics and electronics. *Nat. Mater.* **17**, 618–624 (2018).
21. Li, X. et al. Evaporation-induced sintering of liquid metal droplets with biological nanofibrils for flexible conductivity and responsive actuation. *Nat. Commun.* **10**, 3514–3522 (2019).
22. Parida, K. et al. Extremely stretchable and self-healing conductor based on thermoplastic elastomer for all-three-dimensional printed triboelectric nanogenerator. *Nat. Commun.* **10**, 2158–2166 (2019).
23. Yun, G. et al. Liquid metal-filled magnetorheological elastomer with positive piezoconductivity. *Nat. Commun.* **10**, 1300–1308 (2019).
24. Wang, J. et al. Printable superelastic conductors with extreme stretchability and robust cycling endurance enabled by liquid-metal particles. *Adv. Mater.* **30**, 1706157 (2018).
25. Tang, L. et al. Printable metal-polymer conductors for highly stretchable bio-devices. *iScience* **4**, 302–311 (2018).
26. Yang, Y. et al. Stretchable energy-harvesting tactile interactive interface with liquid-metal-nanoparticle-based electrodes. *Adv. Funct. Mater.* **30**, 1909652 (2020).

27. Zhang, W. et al. Liquid metal/metal oxide frameworks. *Adv. Funct. Mater.* **24**, 3799–3807 (2014).

28. Lin, Y. et al. Handwritten, soft circuit boards and antennas using liquid metal nanoparticles. *Small* **11**, 6397–6403 (2015).

29. Ren, L. et al. Nanodroplets for stretchable superconducting circuits. *Adv. Funct. Mater.* **26**, 8111–8118 (2016).

30. Song, H. et al. Ga-based liquid metal micro/nanoparticles: recent advances and applications. *Small* **16**, 1903391 (2020).

31. Dickey, M. D. et al. Eutectic gallium-indium (EGaIn): a liquid metal alloy for the formation of stable structures in microchannels at room temperature. *Adv. Funct. Mater.* **18**, 1097–1104 (2008).

32. Chiechi, R. C., Weiss, E. A., Dickey, M. D. & Whitesides, G. M. Eutectic gallium-indium (EGaIn): a moldable liquid metal for electrical characterization of self-assembled monolayers. *Angew. Chem. Int. Ed.* **47**, 142–144 (2008).

33. Pan, C. et al. A liquid-metal-elastomer nanocomposite for stretchable dielectric materials. *Adv. Mater.* **31**, 1900663 (2019).

34. Boley, J. W., White, E. L. & Kramer, R. K. Mechanically sintered gallium-indium nanoparticles. *Adv. Mater.* **27**, 2355–2360 (2015).

35. Regan, M. J. et al. X-ray study of the oxidation of liquid-gallium surfaces. *Phys. Rev. B* **55**, 10786–10790 (1997).

36. Suslick, K. S. Sonochemistry. *Science* **247**, 1439–1445 (1990).

37. Li, J. & Kim, J.-K. Percolation threshold of conducting polymer composites containing 3D randomly distributed graphite nanoplatelets. *Compos. Sci. Technol.* **67**, 2114–2120 (2007).

38. Sekitani, T. et al. A rubberlike stretchable active matrix using elastic conductors. *Science* **321**, 1468–1472 (2008).

39. Araki, T., Nogi, M., Suganuma, K., Kogure, M. & Kirihara, O. Printable and stretchable conductive wirings comprising silver flakes and elastomers. *IEEE Electron Device Lett.* **32**, 1424–1426 (2011).

40. Ma, R., Kang, B., Cho, S., Choi, M. & Baik, S. Extraordinarily high conductivity of stretchable fibers of polyurethane and silver nanoflowers. *ACS Nano* **9**, 10876–10886 (2015).

41. Kim, Y. et al. Stretchable nanoparticle conductors with self-organized conductive pathways. *Nature* **500**, 59–63 (2013).

42. Stoyanov, H., Kollosche, M., Risse, S., Waché, R. & Kofod, G. Soft conductive elastomer materials for stretchable electronics and voltage controlled artificial muscles. *Adv. Mater.* **25**, 578–583 (2013).

43. Matsuhsia, N. et al. Printable elastic conductors by in situ formation of silver nanoparticles from silver flakes. *Nat. Mater.* **16**, 834–840 (2017).

44. Ma, R., Lee, J., Choi, D., Moon, H. & Baik, S. Knitted fabrics made from highly conductive stretchable fibers. *Nano Lett.* **14**, 1944–1951 (2014).

45. Park, Y.-G. et al. Three-dimensional, high-resolution printing of carbon nanotube/liquid metal composites with mechanical and electrical reinforcement. *Nano Lett.* **19**, 4866–4872 (2019).

46. Wang, Y. et al. Standing enokitake-like nanowire films for highly stretchable electronics. *ACS Nano* **12**, 9742–9749 (2018).

47. Sun, H., Han, Z. & Willenbacher, N. Ultrastretchable conductive elastomers with a low percolation threshold for printed soft electronics. *ACS Appl. Mater. Interfaces* **11**, 38092–38102 (2019).

48. Wang, Y. et al. A highly stretchable, transparent, and conductive polymer. *Sci. Adv.* **3**, 10–19 (2017).

49. Yao, B. et al. Highly stretchable polymer composite with strain-enhanced electromagnetic interference shielding effectiveness. *Adv. Mater.* **32**, 1907499 (2020).

50. Dang, Z.-M. et al. Fundamentals, processes and applications of high-permittivity polymer–matrix composites. *Prog. Mater. Sci.* **57**, 660–723 (2012).

51. Liang, J. et al. Intrinsically stretchable and transparent thin-film transistors based on printable silver nanowires, carbon nanotubes and an elastomeric dielectric. *Nat. Commun.* **6**, 7647–7656 (2015).

52. Zhang, Z., Du, C., Jiao, H. & Zhang, M. Polyvinyl alcohol/SiO<sub>2</sub> hybrid dielectric for transparent flexible/stretchable all-carbon-nanotube thin-film-transistor integration. *Adv. Electron. Mater.* **6**, 1901133 (2020).

53. Kim, J. O. et al. Network structure modification-enabled hybrid polymer dielectric film with zirconia for the stretchable transistor applications. *Adv. Funct. Mater.* **30**, 1906647 (2020).

54. Feng, P., Zhong, M. & Zhao, W. Stretchable multifunctional dielectric nanocomposites based on polydimethylsiloxane mixed with metal nanoparticles. *Mater. Res. Express* **7**, 015007 (2019).

55. Rao, Y.-L. et al. Stretchable self-healing polymeric dielectrics cross-linked through metal-ligand coordination. *J. Am. Chem. Soc.* **138**, 6020–6027 (2016).

## ACKNOWLEDGEMENTS

The work reported here was supported by NSFC (51872146, 51673099), the “Fundamental Research Funds for the Central Universities,” Nankai University (63191520), and Tianjin Municipal Science and Technology Commission (17JCZDJC30200) in China.

## AUTHOR CONTRIBUTIONS

Y.L. designed, fabricated, characterized the devices, and analyzed the data. X.J. helped with manuscript figures. J.L. conceived of the work and coordinated the research. All authors read and approved the final manuscript.

## COMPETING INTERESTS

The authors declare no competing interests.

## ADDITIONAL INFORMATION

**Supplementary information** The online version contains supplementary material available at <https://doi.org/10.1038/s41528-021-00108-w>.

**Correspondence** and requests for materials should be addressed to X.J. or J.L.

**Reprints and permission information** is available at <http://www.nature.com/reprints>

**Publisher's note** Springer Nature remains neutral with regard to jurisdictional claims in published maps and institutional affiliations.



**Open Access** This article is licensed under a Creative Commons Attribution 4.0 International License, which permits use, sharing, adaptation, distribution and reproduction in any medium or format, as long as you give appropriate credit to the original author(s) and the source, provide a link to the Creative Commons license, and indicate if changes were made. The images or other third party material in this article are included in the article's Creative Commons license, unless indicated otherwise in a credit line to the material. If material is not included in the article's Creative Commons license and your intended use is not permitted by statutory regulation or exceeds the permitted use, you will need to obtain permission directly from the copyright holder. To view a copy of this license, visit <http://creativecommons.org/licenses/by/4.0/>.

© The Author(s) 2021